



ORIGINAL ARTICLE

Nanocomposite scaffolds based on gelatin and alginate reinforced by Zn_2SiO_4 with enhanced mechanical and chemical properties for tissue engineering



Mojgan Ghanbari, Masoud Salavati-Niasari*, Fatemeh Mohandes

Institute of Nano Science and Nano Technology, University of Kashan, Kashan P. O. Box. 87317–51167, Iran

Received 5 November 2021; accepted 21 January 2022

Available online 28 January 2022

KEYWORDS

Injectable scaffold;
 Zn_2SiO_4 ;
Cartilage repair;
Inorganic reinforcement;
Rheological properties

Abstract Hydrogels have been employed in regenerative treatments for decades because of their biocompatibility and structural similarity to the native extracellular matrix. Injectable hydrogels with interconnected porosity and specific internal structures are momentous for tissue engineering. Here, we develop a group of injectable hydrogels comprised of oxidized alginate (OA)/gelatin (GEL) strengthened by modifying the amount of Zn_2SiO_4 nanoparticles. The physicochemical characteristics of OA/GEL/ Zn_2SiO_4 hydrogels were studied by mechanical strength, swelling ratio, and morphology. The outcomes revealed that the mechanical characteristics of hydrogels containing a higher amount of Zn_2SiO_4 (0.12 wt%) improved more than five times than the hydrogels fabricated without Zn_2SiO_4 . The *in vitro* degradation outcomes manifested the degradation of the hydrogel comprising 0.12 wt% Zn_2SiO_4 NPs was slower than one without NPs, and remaining masses of hydrogels depend on different contents of Zn_2SiO_4 NPs. The hydrogel containing Zn_2SiO_4 NPs exhibited less cytotoxicity and good cell attachment than the hydrogels prepared without the nanoparticles. The cell viability and attachment show that the nanocomposite hydrogels are biocompatible (>96%) with great cell adhesion to osteosarcoma cell line MG63 depending on the presence of Zn_2SiO_4 . The superior physical, chemical as well as mechanical characteristics of the hydrogels containing Zn_2SiO_4 NPs along with their cytocompatibility suggest that they can introduce as good candidates as scaffolds in tissue engineering.

© 2022 The Author(s). Published by Elsevier B.V. on behalf of King Saud University. This is an open access article under the CC BY-NC-ND license (<http://creativecommons.org/licenses/by-nc-nd/4.0/>).

* Corresponding author.

E-mail address: salavati@kashanu.ac.ir (M. Salavati-Niasari).

Peer review under responsibility of King Saud University.



1. Introduction

Growth disorders, joint damage, and aging cause loss of mobility and joint injury since the natural joint does not have a source of blood to help natural self-healing (Ochi et al., 2001; Yan et al., 2016). Conventional treatments, including medication and organ transplantation, possess shortcomings of side effects and lack of organ supply, respec-

tively (Temenoff & Mikos, 2000). Lately, tissue engineering affords an inherent treatment to reconstruct tissue injuries with the most encouraging procedures of autogenic cell/tissue transplant in surgical operation (Tan et al., 2014). In this manner, in situ forming gel frameworks are injected into the injury sections to repair joint functions and improved cartilage and bone reconstruction, which contribute a suitable condition for the transfer of living cells (LeBaron and Athanasiou, 2000).

Injectable and in situ forming hydrogels are broadly used in cartilage tissue engineering because of its notable benefits of relationships to the extracellular matrix (ECM), providing unusual imperfections to be supplied with and simple at the combining cells via facile blending (Gheysari et al., 2020; Tan et al., 2012; Yan et al., 2014). Hydrogels are typically accepted as an injectable scaffold matrix since they are easily implanted by a needle to obtain minimally invasive therapy (Tan et al., 2013). Additionally, 3D hydrogel networks have the benefits of absorbing a high volume of water to create a swelling framework instead of being crumbled (Balakrishnan & Jayakrishnan, 2005).

Injectable hydrogels, each synthetic or natural, can be injected in fluid–structure and consequently cross-linked with chemical or physical cross-linkers. In situ formable self-crosslinking hydrogels are quickly managed by minimally invasive transfer (Ketabat et al., 2017; Liow et al., 2016b; Naghizadeh et al., 2018). The in situ gelation and injectability of the hydrogels, as well as their minimally invasive characteristic, enhance patient convenience (Balakrishnan et al., 2014; Liow et al., 2016a). Natural scaffolds have a greater impact on cell adhesion, division, and migration correlated to synthetics (Dou et al., 2014). Sodium alginate or alginic acid (AL) is a water-soluble, linear polymer driven of seaweed and comprises of alpha-L-guluronic acid and beta-D-mannuronic acid blocks. Alginate and its derivatives are widely employed in cartilage tissue engineering owing to high viscosity, stability, and the gelation ability in aqueous solutions. Besides, oxidized alginates (OA) provide further functional groups and a quicker degeneration degree for controlled drug delivery (Fan et al., 2011). In addition, natural proteins, including gelatin are broadly utilized in drug delivery and tissue engineering because of its high-grade biodegradation, biocompatibility and cell attachment (Chen et al., 2017; Gheysari et al., 2020; Karvandian et al., 2020). In spite of their numerous benefits, the hardness of hydrogels is usually twice less than cartilage (100–1000 kPa) (Levental et al., 2007). These weak mechanical attributes restrict their utilization of space-filling frameworks applied for the transfer of cells and bioactive compounds.

In tissue engineering, one of the most promising challenges is to provide living constructs that can integrate with the surrounding tissues. Over the past years, different types of scaffolds and bioreactors have been designed to overcome the limitations related to the static culture systems, such as limited diffusion and inhomogeneous cell-matrix distribution (D'Amora et al., 2016). As already recognized, scaffolds should possess a set of chemical, biochemical and morphological cues to promote and control specific events at the cellular and tissue levels. On the contrary, the ideal feature of a bioreactor is that it should supply suitable levels of oxygen, nutrients, cytokines, growth factors, and mechanical stimulation for cell migration and scaffold colonization. A valuable candidate for tissue engineering applications should be a 3D additive-manufactured scaffold, which could satisfy the above reporting requirements. It will provide a morphologically controlled and tailored structure with interconnected pores of different sizes (D'Amora et al., 2017; De Santis et al., 2015; Gloria et al., 2020).

So far, various approaches have been promoted to improve the mechanical characteristics of hydrogels, for instance, concentration of polymer, polymerization degree, along with particles, fibers embedding, or carbon nanotubes (Boyer et al., 2018). It has been proven that the reinforcement of natural polymers with inorganic nanostructures can improve the mechanical behaviors of the hydrogels (Radhakrishnan et al., 2015; Wu et al., 2016). Generally, bioactive ceramics such as bioactive glasses (BG) (Sergi et al., 2020), LAPONITE® (Eslahi et al., 2016), SiO₂ NPs (Zaragoza & Asuri, 2019) with

superior bioactivity and biocompatibility, have been used as reinforcements to improve the mechanical characteristics of hydrogels (Rahaman et al., 2011). Very recently, Emami et al. (Emami et al., 2021) found that hydroxyapatite NPs enhance rheological and toughness properties of gelatin/oxidized alginate hydrogels when used as bone scaffolds. Several researches focused on gelatin/alginate hydrogels reinforced with TiO₂ and tricalcium phosphate (TCP) (Urruela-Barrios et al., 2019) as well as graphene oxide (GO) (Purohit et al., 2020) showed enhanced mechanical properties. So far, there are a few inorganic components, for instance, carbon nitride quantum dots (Ghanbari et al., 2021a), layered double hydroxides (Fu et al., 2010; Hu & Chen, 2014; Nourafkan et al., 2017), clay minerals (Chen et al., 2004; Okay & Oppermann, 2007; Tjong, 2006), zirconium oxide nanoparticles (NPs) (Ghanbari et al., 2021), metal oxide NPs (Al-Nayili and Albdiry 2021; Kadhem and Al-Nayili, 2021; Al-Nayili, et al., 2021; Bhardwaj et al., 2008), silica nanoparticles (Wang et al., 2012), carbon nanotubes (Zhang et al., 2009), and nitrogen-doped carbon dots (Ghanbari et al., 2021b) have been studied on mechanical and chemical properties of hydrogels. Herein, Wilmette (Zn₂SiO₄), an inorganic zinc-rich silicate bioceramic that possesses a chemical composition comparable to minerals found in native bone composition (Amiri et al., 2016; Ardeshiryajimi et al., 2013; Jamshidi Adegani et al., 2014), is introduced as reinforcement to enhance the mechanical features of OA/GEL hydrogels. In this research, a group of biodegradable and biocompatible injectable hydrogel combination systems, namely Oxidized Alginate/Gelatin (OA-GEL) by adding zinc silicate nanoparticles as a reinforcement (Zn₂SiO₄ NPs) has been reported. A comparative study was done with the same. The mechanical strength, swelling ratio and biodegradation were studied to obtain an optimum and stable hydrogel. The as-synthesized hydrogels cross-linked using N-hydroxysuccinimide (NHS) and 1-ethyl-3-(3-dimethylaminopropyl) carbodiimide (EDC) including Zn₂SiO₄ nanostructures can be apply for the reconstruction of cartilage and bone, wherever the hydrogel precursors provide efficacy in nutrients, the facility of injection, cell transport, cytocompatibility, generation, and cell adhesion.

2. Materials and methods

2.1. Materials

Sodium alginate (low viscosity derived from brown algae), potassium periodate, ethylene glycol, ethanol, n-propanol, gelatin (type B from bovine skin), zinc nitrate hexahydrate (Zn(NO₃)₂·6H₂O), silver nitrate (AgNO₃), sodium chloride (NaCl), acetone, tetraethyl orthosilicate (TEOS), N-hydroxysuccinimide (NHS), 1-Ethyl-3-(3-dimethylaminopropyl) carbodiimide (EDC), Ethylene glycol (EG), tetraethylpentamine (TEPA) were acquired from Merck and Sigma-Aldrich Company and employed without additional refinement.

2.2. Alginate oxidation

2.01 g of sodium alginate and 11.2 ml of n-propanol were blended with DI-water in a 250-mL beaker to obtain 225 ml in total. The mix was kept at 30 °C in the dark under stirring (5 h) to dissolve alginate completely. 1.16 g of Potassium periodate (KIO₄) dispersed in 30 ml DI-water was combined with alginate solution. The mixture was kept in the dark for 24 h. The reaction was quenched by adding 1 ml of Ethylene glycol (EG), and the mix was agitated for another 30 min. 6.5 g of Sodium chloride (NaCl) was dissolved in the above suspension to purify the polymer, which was next gently added to 400 ml agitated ethyl alcohol. The white precipitate was dissolved in

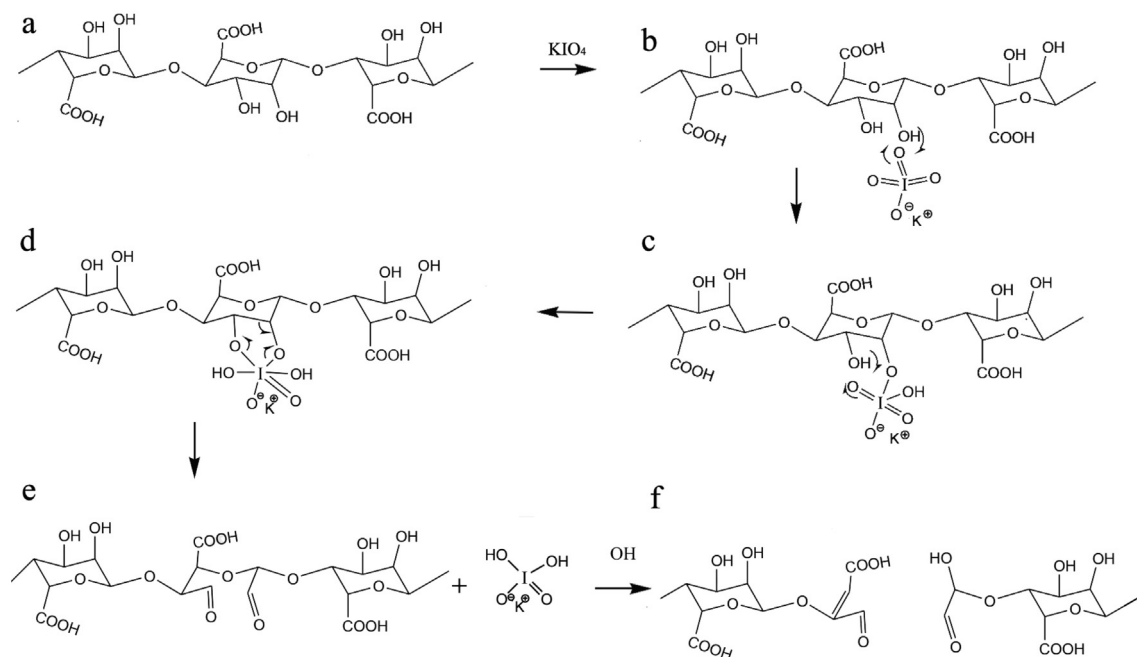


Fig. 1 Mechanism of oxidation alginate by KIO₄.

DI-water with 3.3 g of NaCl and reprecipitated in 250 ml ethyl alcohol. The precipitate was dissolved in DI-water again and precipitated in 200 ml acetone. Eventually, the precipitate was rinsed in agitated ethyl alcohol for 15 min, refined, and dried at 25 °C (Rogalsky et al., 2011). The lack of periodate was controlled by combining 500 μ L fractional of the dialyate to 500 μ L of a 1% silver nitrate solution, and assuring the nonexistence of any precipitate (Balakrishnan & Jayakrishnan, 2005). Fig. 1 shows the oxidation mechanism of alginate to oxidized alginate.

2.3. Synthesis of zinc silicate (Zn₂SiO₄) nanostructures

Zn₂SiO₄ nanostructures were fabricated by the reaction within TEOS and Zn(NO₃)₂·6H₂O with a stoichiometric ratio of 2:1 under sonication. In summary, 1.0 ml of TEOS was dissolved in 10.0 ml of ethanol. The mixture was combined with the beaker containing zinc nitrate and stirred for 10 min. Following, diluted TEPA was added dropwise to the mentioned solution (pH was set on 10) below ultrasound for 15 min. The white powder was filtered and rinsed with ethanol three times and calcined at 900 °C for 2 h.

2.4. Preparation of OA/GEL/Zn₂SiO₄ hydrogels

In a typical procedure, 4 ml of 6 wt% of OA solution was agitated with 4 ml of 15 wt% of GEL at 37 °C. The cross-linker, including a mixture of 0.1 g EDC and 0.05 g NHS, was added to the above solution. The first gelation was observed in 4–5 s and kept at 37 °C, resulting in the creation of a perfect gel after 2 min. Different weight percentages of Zn₂SiO₄ (0.12, 0.06, and 0.03 wt%) was added to the 4 ml of 6 wt% of OA solution and agitated for 5 min. Next, 4 ml of 15 wt% of GEL was added to the suspension and stirred for another 5 min. The final solutions were mixed for 2 min by adding EDC and NHS as

cross-linker agents. The samples were freeze-dried for 30 h. Three-dimensional scaffolds with a diameter of about 2 cm and a thickness of 1 cm were produced.

2.5. Swelling behavior and degradation

The water absorption of hydrogels was evaluated by the gravimetric technique. Approximately 0.2 g (M_0) of the scaffolds were incubated in 12 ml PBS (pH = 7.4) for one day to accomplish equivalent swelling. The floating solution was removed, and the swollen scaffold was weighed (M_s) (Karvandian et al., 2020):

$$SR(\%) = (W_s - W_0) / W_0 \times 100 \quad (1)$$

Mass degradation/erosion degrees were additionally evaluated likewise at various periods up to 21 days. All tests were accomplished five times.

2.6. Materials characterizations

Fourier transform infrared spectroscopy (Shimadzu Varian 4300 spectrophotometer) was utilized to investigate the chemical composition of oxidized alginate and the fabricated hydrogels applying KBr pellets in the wavenumber between 4000 and 400 cm^{-1} . A field emission scanning electron microscopy (TESCAN MIRA 3 FE-SEM) was used to study the morphological and structural of lyophilized hydrogels. The lyophilized hydrogels were cross-sectioned, coated by gold (Au), and detected by FE-SEM at an accelerating voltage of 15 kV. High-resolution transmission electron microscopy (EM 208, Philips HR-TEM with an accelerating voltage of 100 kV) was utilized to observe carbon nitride quantum dots. A Physica MCR 300 Rheometer (Anton Paar Ltd., Austria) was utilized to measure the oscillatory rheological properties of the hydrogels.

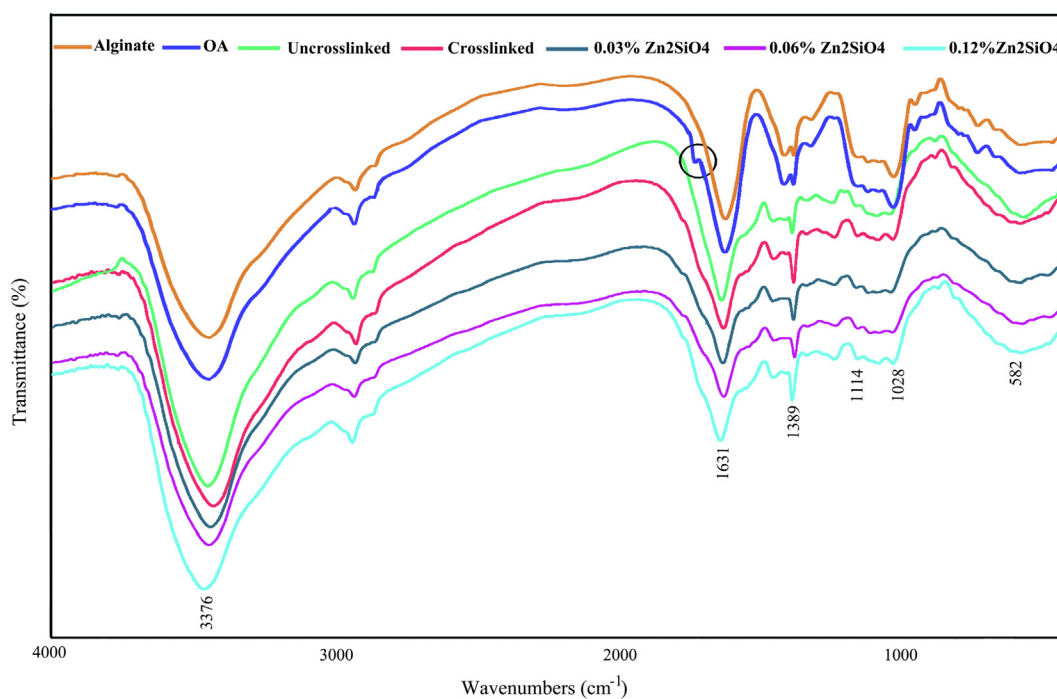


Fig. 2 FTIR spectrum of alginate, oxidized alginate, and the hydrogels containing Zn_2SiO_4 NPs.

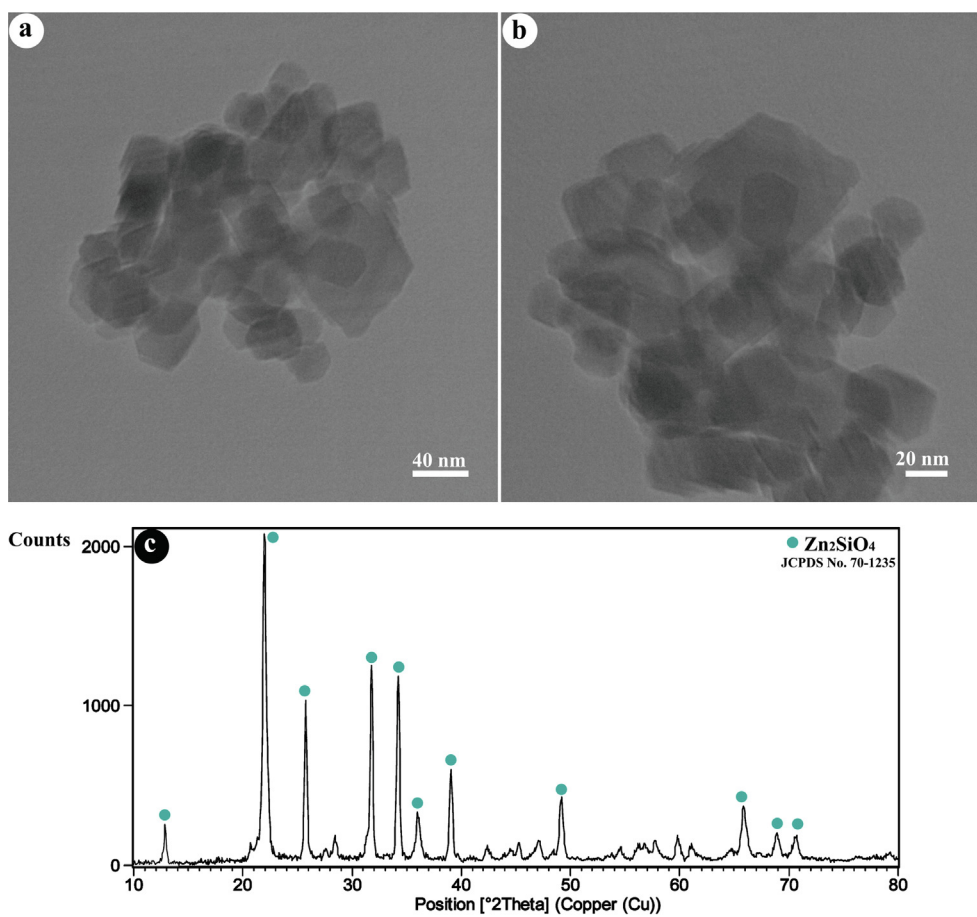


Fig. 3 (a,b) TEM images, and (c) XRD pattern of as-fabricated Zn_2SiO_4 NPs.

2.7. Mechanical properties

A Rheometer (Physica MCR 300, Anton Paar Ltd., Austria) was applied to evaluate the rheological characteristics of scaffolds employing a parallel plate of a round disc with a gap of 0.5 mm and a diameter of 25 mm. An amplitude sweep was directed at a constant angular frequency of 1 Hz to determine the boundary of linear viscoelastic behavior. The strain amplitude was held at 0.1% throughout the experiment. The participation of the solid-like form (storage modulus (G')) and liquid-like form (loss modulus (G'')) were recorded by temperature sweep in the range of 20–50 °C at a rate of 1 °C/min to evaluate temperature of gelation. Angular frequency was 1 Hz. Every following rheological experiment was carried out under simulated physiological circumstances (at 37 °C in PBS pH = 7.4), according to the possible use of scaffolds. The oscillatory rheological measurement as a time function was carried out at a constant frequency of 1 Hz to estimate the gelation time. The gelation time or gel point was designated as the time that the storage modulus (G') and loss modulus (G'') were equal (Macaya et al., 2011). The scaffolds were swollen in 2 ml PBS for 1 h and transferred to the rheometer platform. Following, frequency sweep analyses were conducted in the linear viscoelastic region to determine the dynamic viscoelastic behavior at 37 °C on a wide range of frequencies (0.1–100 Hz).

2.8. In vitro biological assays

In vitro biocompatibility of the hydrogels was estimated utilizing 3-(4,5-dimethylthiazol-2-yl)-2,5-diphenyltetrazolium bromide (MTT assay), which depends on the mitochondrial MTT reduction to produce an insoluble dark blue formazan production. The samples were incubated in 1 ml of RPMI 1640 culture medium (Sigma-Aldrich) at 37 °C supplied by 10% (w/w) fetal bovine serum (FBS) for 24 and 72 h to achieve the extracts of the as-dried hydrogels. The growth medium (RPMI and FBS) was utilized as the control under similar conditions. The MG63 cells were cultivated in 96-well plates at a density of 1×10^4 MG63 cells per sample. The growth medium was substituted by the hydrogels extract. The extract was removed after 24 h. 100 μ L of the MTT solution (0.5 mg/mL) was added to all wells and incubated for another four hours at 37 °C. Then, the solution was eliminated, and 100 μ L isopropanol was consequently added to liquefy the MTT crystals. The absorbance of the solutions was measured with a microplate spectrophotometer (Biotek Powerwave XS2, USA) at 570 nm.

In order to study the architecture of the cells attached to the hydrogels, cross-section SEM images of the samples have been recorded. The hydrogels were put in a Petri dish, and incubated in the existence of DMEM and MG63 cells at 37 °C for 24 h. After incubating, the hydrogels were rinsed multiple

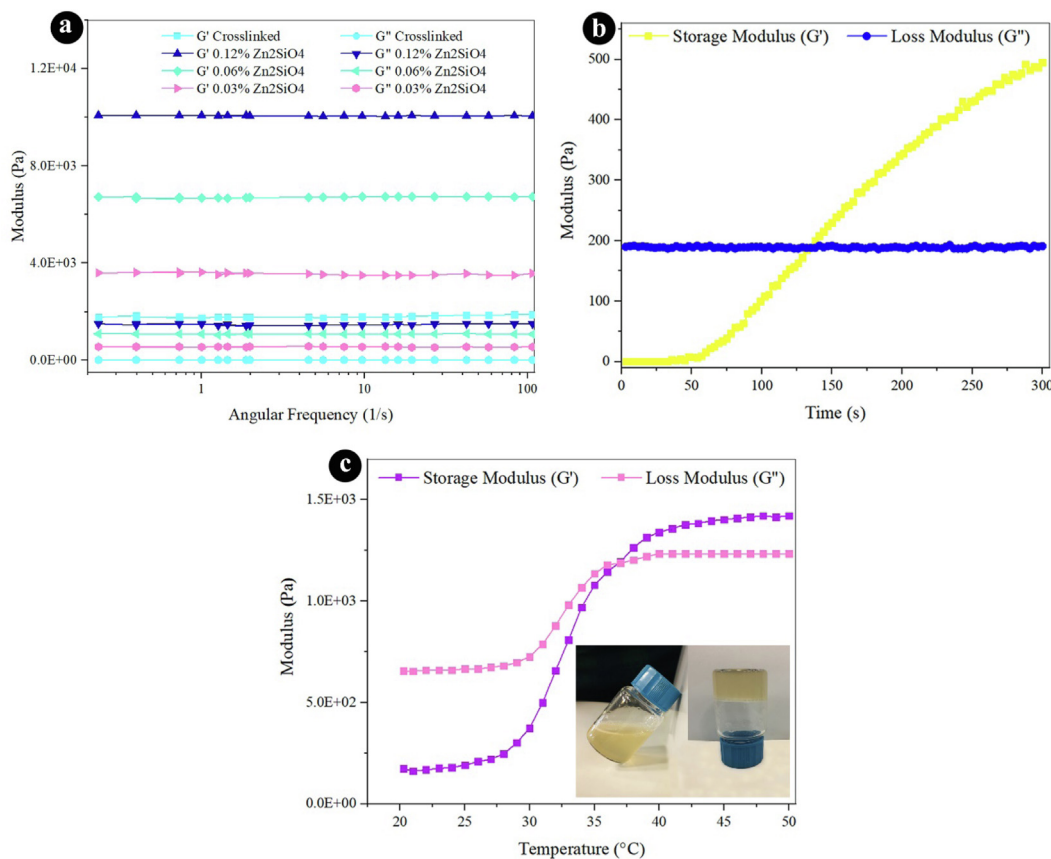


Fig. 4 Rheological properties (a) frequency sweep at 37 °C for all hydrogels, (b) time sweep at 37 °C, and (c) temperature sweep for crosslinked hydrogel.

times by PBS and set by 2.5% glutaraldehyde solution for 4 h at 4 °C. Eventually, the samples were lyophilized and coated with Au for FESEM surveys.

3. Result and discussion

3.1. FTIR data

FTIR spectroscopy is applied to study the various functional groups existence and the type of chemical bonds in the structure (Ul-Islam et al., 2012). Hence, the FTIR spectra of AL, OA, and their composite scaffolds were conducted to confirm the existence of gelatin, alginate, and their chemical crosslinking in the injectable hydrogel. The FTIR spectra of OA, AL, and the composite hydrogels are presented in Fig. 2, designating several bands of multiple functional groups. This spectrum showed a specific band for –OH stretching vibration at 3376 cm^{-1} from alginate (Aljohani et al., 2018). The other small band at 3406 cm^{-1} , somewhat overlaid by –OH stretching, was allocated to the N–H stretching of gelatin. The broad absorption band at 3410 cm^{-1} , ascribed to O–H and N–H stretching, moved to a lower wavenumber at 3376 cm^{-1} , showing an increment in the hydrogen bonding. These differences are comparable to the previous studies (Majidi et al., 2018) and designate good molecular compatibility and the presence of intermolecular interplays among gelatin and alginate. The presence of the aldehyde group (–CHO) was confirmed at

1723 cm^{-1} . In some cases, this peak is not identified due to the hemiacetal configuration of –OH groups with free –CHO groups on the nearby D-glucuronic acid subunits (Jejurikar et al., 2012; Vieira et al., 2008). The specific absorption peaks between 1000 and 1700 cm^{-1} were allotted to different functional groups of gelatin and alginate. The bands at 1631 and 1389 cm^{-1} were assigned to asymmetric and symmetric stretching vibrations of carboxylic acid, respectively of alginate. The band at 1114 cm^{-1} was allocated to N–H bending mode of gelatin (Khan et al., 2016; Luo et al., 2015). The absorption band at 582 cm^{-1} is related to symmetric stretching vibration of Zn–O (Chandra Babu et al., 2017). The Zn_2SiO_4 bonds overlay with characteristic bands of AL and GEL and are not observable in the spectra because of the low content of Zn_2SiO_4 in the hydrogel system. Based on the proposed cross-linking mechanism of OA and GEL chains, the aldehyde groups within the OA chain covalently bind to amine groups of lysine and hydroxylysine in gelatin through Schiff base formation, allowing the fabrication of three-dimensional (3D) scaffolds (Sarker et al., 2017).

3.2. Characterization of Zn_2SiO_4

Fig. 3(a-b) reveals the TEM images of ZnO NPs. As can be seen, nanoparticles in the range of 20–60 nm with an average diameter of ≈ 36 nm are composed. The XRD pattern of Zn_2SiO_4 is in perfect agreement with the Rhombohedral structure of willemite with the reference code of 70–1235 (Fig. 3c).

Table 1 Rheological properties and pore size of the hydrogels at 37 °C and frequency of 1 Hz.

Sample	Storage modulus (Pa)	Loss modulus (Pa)	Pore size (μm)	Ref
Crosslinked 0.00 wt% Zn_2SiO_4	1801 \pm 83	11.52 \pm 0.32	216.7	This work
0.03 wt% Zn_2SiO_4	3565 \pm 65	555 \pm 24	166.3	This work
0.06 wt% Zn_2SiO_4	6720 \pm 70	1068 \pm 28	164.4	This work
0.12 wt% Zn_2SiO_4	10074 \pm 24	1466 \pm 41	139.3	This work
Crosslinked OA/GEL by Borax contain 10 wt% HAP	6600	–	–	(Emami et al., 2021)

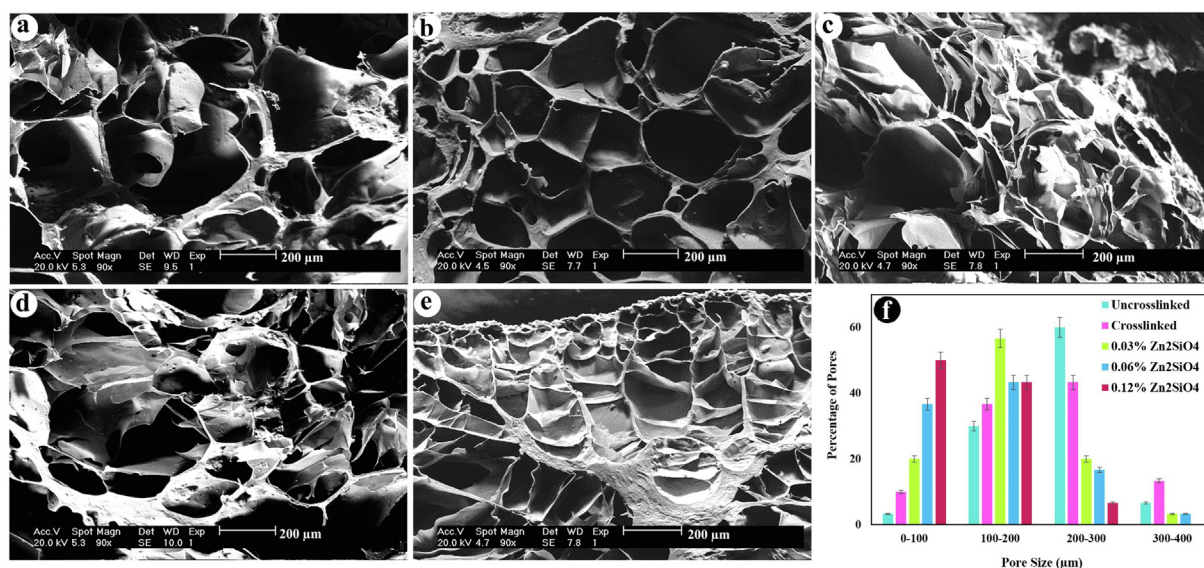


Fig. 5 Cross-section morphology of freeze dried hydrogels (a) uncrosslinked, (b) crosslinked, (c) containing 0.03 wt% Zn_2SiO_4 , (d) 0.06 wt% Zn_2SiO_4 , (e) 0.12 wt% Zn_2SiO_4 , and (f) pore size distribution diagram of the hydrogels ($p < 0.01$).

3.3. Rheological properties

The rheological characteristics of nanocomposite hydrogels were determined via a frequency sweep technique to investigate the viscoelasticity. As presented in Fig. 4a, all the samples showed similar linear rheological performances. The loss modulus (G'') and storage modulus (G') were improved by expanding the quantity of Zn_2SiO_4 . The G' was higher than G'' with a kind of significance for all the hydrogels across the entire frequency range, which designated the durability of the 3D network in the hydrogel through the Schiff-base reaction. Besides, it was remarked that the addition of strengthening material to adjust the viscoelastic behavior of the hydrogels at higher amount of Zn_2SiO_4 became more effective than low amounts (Fig. 4a and Table 1). The addition of Zn_2SiO_4

not only improves G' of hydrogels by more than fivefold but also boosts the G'' notably. It could be noticed that G' increments quickly with the extended Zn_2SiO_4 content, presumably because of the increment in the crosslinking degree, which reduces the movement of macromolecular chains. By comparing the G' values of OA/GEL hydrogels reinforced by 10 wt% of hydroxyapatite NPs (Emami et al., 2021) and 0.06–0.12 wt% of Zn_2SiO_4 NPs, it was found that low concentrations of Zn_2SiO_4 NPs are more effective to improve the mechanical properties of the scaffolds.

The time of gelation is one of the major parts of the injectable hydrogels for their usage. The time sweep of the hydrogel was carried out to examine the gelation operation at 37 °C (human body temperature). Prior to gelation, the storage modulus is less than the viscous modulus, which indicates a solution behavior and the dominant viscous properties when the gela-

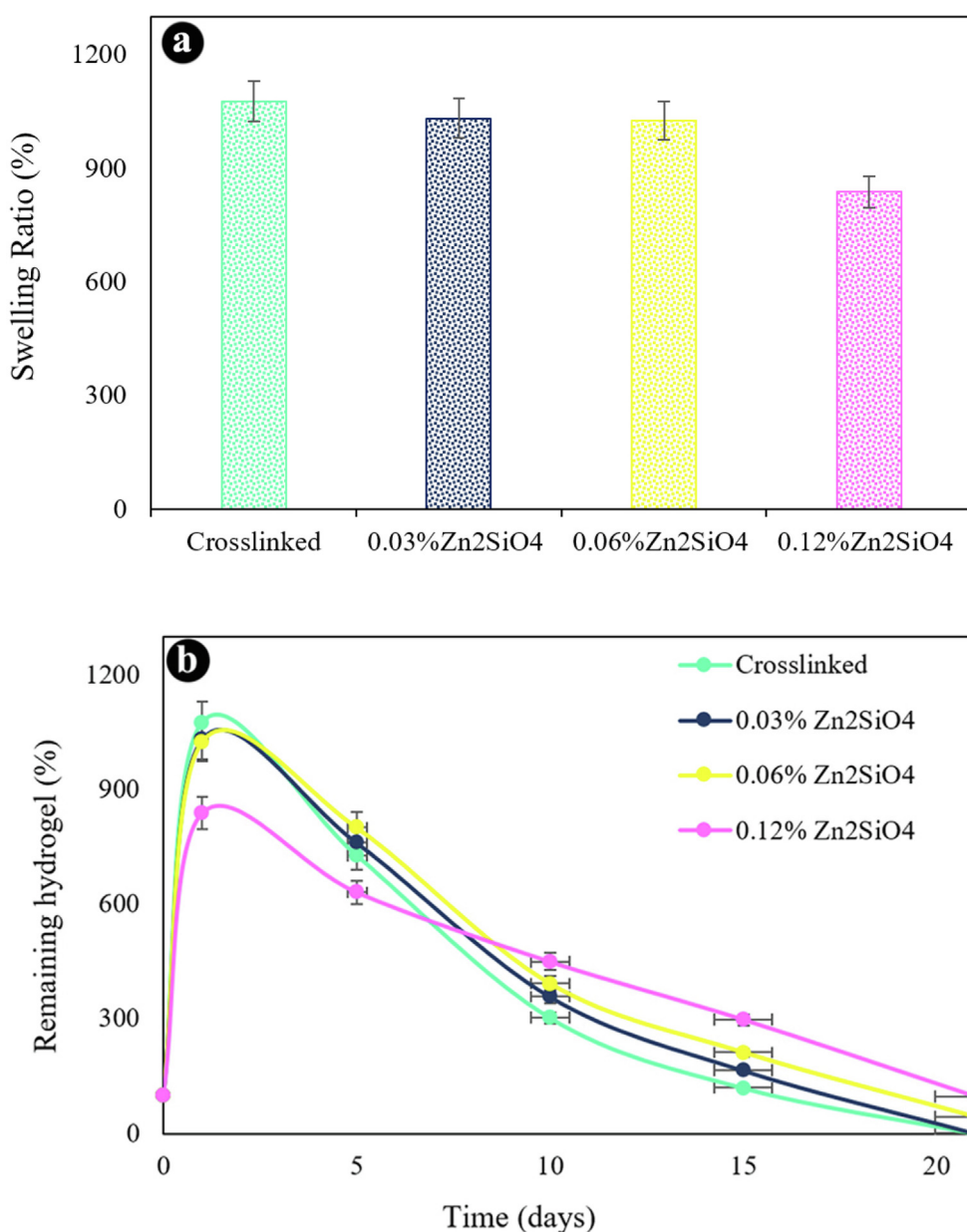


Fig. 6 (a) Swelling ratio of the hydrogels, (b) *in vitro* biodegradation after various incubation times in PBS at 37 °C.

tion is started. G' progresses faster than G'' by increasing the time. This means that the liquid phase has turned into a jelly phase with excellent elasticity. The time of gelation is 2 min (120 s), which is sufficient for operating as an injectable hydrogel.

Fig. 4c presents the thermosensitive performance of cross-linked scaffold. The temperature was boosted from 20 to 50 °C within a rate of 2 °C/min. The G'' and G' values were drawn versus temperature in Fig. 4c. G' is less than G'' at the lower temperature, while the G' amounts are higher than the corresponding G'' values at the higher temperature. The gelation temperature can be determined by the crossover of G' and G'' as presented in Fig. 4c. The data verify that the gelation temperature of the hydrogel is 37 °C. This suggests that human body temperature can change liquid to gel.

3.4. Morphology of microstructures

As presented in Fig. 5, the SEM images exhibit the microstructure of the nanocomposite hydrogels among different concentrations of Zn_2SiO_4 . The microstructure of all hydrogels manifested a porous structure. The interior architecture of the hydrogels is strictly correlated to the Zn_2SiO_4 content.

The pore size reduces with increasing the content of Zn_2SiO_4 because of increasing crosslink density and the decrease in the distance among polymer chains. The pore size distribution was estimated by digimizer software and the average pore size was irregular for all scaffolds ranging from 139 μm (cross-linked with 0.12% of Zn_2SiO_4) to 216 μm (uncrosslinked), which is suitable for tissue engineering (Lien et al., 2008).

3.5. Swelling and degradation

Fig. 6a exhibits the swelling degree of the nanocomposite hydrogels after 24 h. The swelling capability of hydrogels is lessened by adding Zn_2SiO_4 NPs. The hydrogel without reinforcement possesses the highest swelling degree (1076%) in 24 h. The hydrogels comprising 0.03 wt% to 0.12 wt% of Zn_2SiO_4 unveiled a swelling ratio of decreasing from 1031 to 838%, sequentially. The small decrease was recognized in the swelling degree by growing the quantity of Zn_2SiO_4 NPs owing to the straight interaction amongst the hydrogel network and Zn_2SiO_4 .

Fig. 6b shows *in vitro* degradation of scaffolds over incubation time in PBS at 37 °C. The amount of Zn_2SiO_4 NPs had a notable impact on mass loss. The hydrogel without Zn_2SiO_4

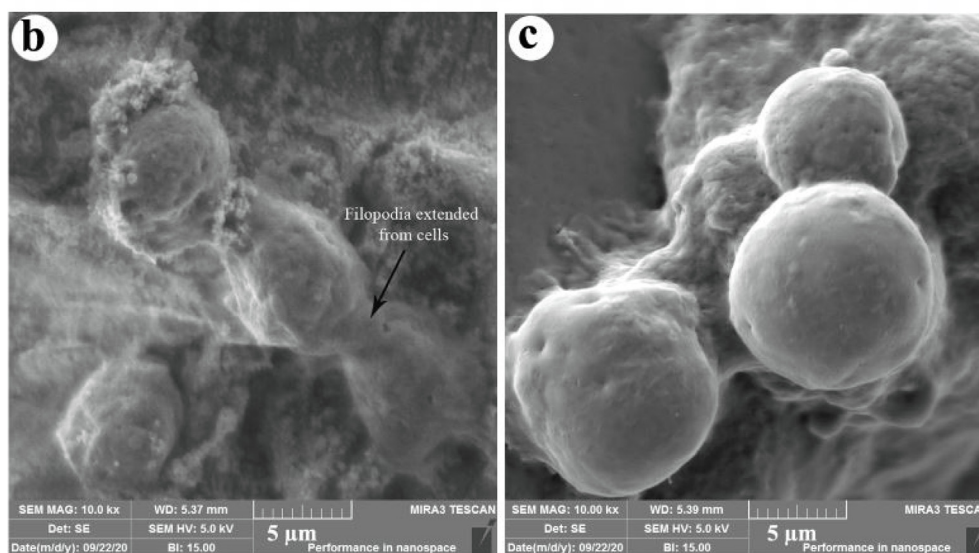
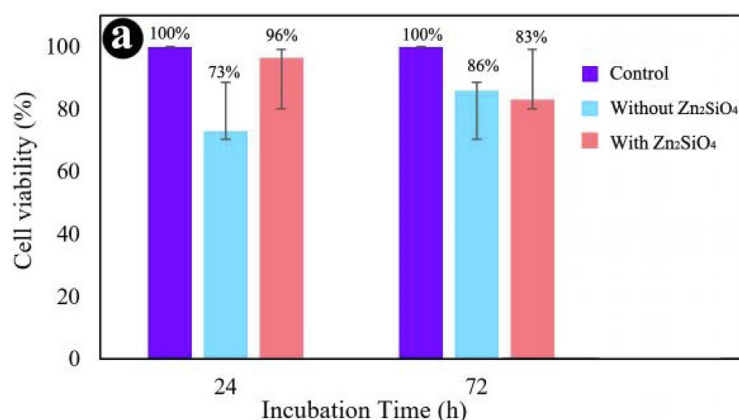


Fig. 7 (a) Cell viability of hydrogels with and without Zn_2SiO_4 NPs, FE-SEM images of cell-cultured hydrogels (b) with 0.12 wt% Zn_2SiO_4 , and (c) without Zn_2SiO_4 .

exhibited a quicker mass loss because of larger pore sizes and destroyed in 21 days. The hydrogels containing 0.06% and 0.12% Zn₂SiO₄ remained up to 21 days. The hydrogel comprising higher NPs content degraded slower than hydrogel with lower Zn₂SiO₄ content. On day 21, the mass residual degree of 0.06 and 0.12 wt% Zn₂SiO₄ hydrogels was 43% and 97%, respectively. The existence of Zn₂SiO₄ drives to an enhanced the density of crosslinking. We selected the nanocomposite scaffold containing 0.12 wt% Zn₂SiO₄ as an ideal hydrogel for further experiments.

3.6. Cell viability and attachment

The first step in examining the cytocompatibility of biomaterials is the MTT assay, which is a fast, sensitive, regulated, and low-priced approach for determining cell proliferation and viability or either a substance comprises notable amounts of biologically toxic extracts. The impact of crosslinked hydrogel and the hydrogel containing 0.12 wt% Zn₂SiO₄ on cytotoxicity of MG-63 cells was studied by the MTT assay after 24 and 72 h. The cell viability of MG-63 cells on the hydrogels is demonstrated in Fig. 7. According to the results of the cyto-

compatibility test, the cell viability of crosslinked hydrogel was 73% and 86% after 24 and 72 h, respectively, while the hydrogel containing 0.12 wt% Zn₂SiO₄ exhibited higher cell viability (96.5% and 83% after 24 and 72 h) than the hydrogels without NPs. Hence, the hydrogels containing 0.12 wt% Zn₂SiO₄ was not toxic to the MG-63 cells and could be applied for bio-applications. The SEM images of the cell attachment on the scaffolds without and with without Zn₂SiO₄ NPs after 4 h incubation are illustrated in Fig. 6(b-c). The cells on cross-linked hydrogel without NPs were attached in spherical form, while the cells attached to the hydrogel containing 0.12 wt% Zn₂SiO₄ was more durable among groups of cells. The presence of filopodia extended from the cells to the hydrogel substrate is shown in Fig. 7b, indicating the cell attachment to the hydrogels. Furthermore, cell attachment to the hydrogel with NPs was notably developed in the presence of Zn₂SiO₄ NPs, due to the interaction of NPs and cells. Table 2 reviews the different hydrogels and their properties obtained for tissue engineering. As demonstrated in this Table, OA/GEL/Zn₂SiO₄ hydrogels are comparable with other composites reported in the literature and are less toxic than the cellulose–alginate and Alginate-PVA-hydroxyapatite hydrogels.

Table 2 Different precursors and their characteristics obtained for tissue engineering.

Materials	Cells	Cell culture	Special	References
Oxidized alginate-gelatin-Zn₂SiO₄	Osteosarcoma cell line MG63	1–3 days	Viability = 97% after 3 days, adding Zn ₂ SiO ₄ increases cell viability, cell attachment, and storage modulus.	This work
Nano-fibrillated cellulose–alginate	Fibroblasts, human nasoseptal chondrocytes	7 days	Cell proliferated with increased viability of ~ 85.7% in contrast to ~ 72.8% on first day, cellulose in fibrillated form enables shear-thinning capability	(Markstedt et al., 2015)
Alginate-PVA-hydroxyapatite	Mouse calvaria (MC) 3 T3-E1	14 days	In vitro, viability = ~77% (after incubation) > ~22% for only alginate, could endure structure for at least 14 days. Alginate hydroxyapatite had optimum mechanical, rheological and biological characteristics, PVA- hydroxyapatite modulates viscosity thus enhancing osteoconduction and viscosity	(Bendtsen et al., 2017)
Na alginate-collagen or Na alginate-agarose	Chondrocytes from the articular cartilage of rats	14–21 days	Na alginate-collagen superior mechanical strength and bioactivity than other combination	(Yang et al., 2018)
Alginate-PVA-hydroxyapatite-collagen	Mouse calvaria (MC) 3 T3-E1	10 days	In vitro, initial viability > 98%, collagen increases cell adhesion and activity	(Bendtsen & Wei, 2017)
Alginate-PLA short fibers	Human chondrocytes	14 days	In vitro, ~80% viability	(Kosik-Kozioł et al., 2017)
Alginate-PCL	Human nasal septum cartilage chondrocytes	7 days	Osteogenic tissue eng., viability = ~94% (chondrocytes) ~ 96% (osteoblast), no observable proliferation in chondrocytes	(Shim et al., 2012)
Alginate-alginate sulfate	bone morphogenetic protein-2, MC3T3-E1	7 days	In vitro, 80% proliferation, improved retention of proteins, alginate-alginate sulfate tightly bound BMP-2, which aids adhesions and cell viability, Ca presence and porosity-favorable for bone tissue engineering	(Park et al., 2018)
Alginate-PCL	Chondrocytes	28 days	In vivo, PCL obstructs the growth of tissues, TGFβ growth factor for biological assistance	(Kundu et al., 2015)
Na alginate-gelatin	Rat Schwann cell line (RSC96)	14 days	Viability = ~93% (post 14 days), printed structures start degrading after 14 days	(Li et al., 2018)
Alginate-PCL	Chondrogenic cell ATDC5	21 days	In vivo, ~70 viable cells, maintained integrity of the PCL scaffold even after 21 days, composite mimics the natural characteristics of cartilage	(Olubamiji et al., 2017)
Alginate-gelatin-fibrinogen	Glioma cells/stem cells	21 days	3rd week showed accelerated growth mimicking the tumor spreading and growth, cell viability = 86.92%	(Dai et al., 2016)

4. Conclusion

The injectable and biodegradable oxidized alginate/gelatin/Zn₂SiO₄ nanocomposite hydrogels have been crosslinked via EDC/NHS as chemical crosslinking agents. Zn₂SiO₄ was homogeneously dispersed in the hydrogel networks and had good impacts on stabilization of the hydrogel networks, increasing mechanical properties, and hindering the weight loss through decreasing swelling ratio. The hydrogels containing a higher amount of Zn₂SiO₄ (0.12 wt%) showed improved mechanical strength, lower swelling ratio, and less weight loss than the hydrogels synthesized without Zn₂SiO₄. The porous structure of the hydrogels exhibited interconnected pores in the range of 139–216 μm. *In vitro* cell seeding on the hydrogels including the NPs revealed higher viability through the culture time of 24 to 72 h than the hydrogels without NPs. The outcomes of the MTT assay also revealed that the hydrogels were not toxic to the cells and not only improved cell proliferation but also retained the cell viability at a reasonable level (> 96%). Since the method of organic/inorganic composite hydrogel structure is attainable and usually conducted below moderate conditions by developing bioactive and mechanical properties, we conclude that these injectable hydrogels will possess promising applications in drug delivery, cartilage and bone tissue engineering.

CRedit authorship contribution statement

Mojgan Ghanbari: Investigation, Formal analysis, Methodology, Writing – review & editing, Writing – original draft, Software. **Masoud Salavati-Niasari:** Investigation, Writing – original draft, Writing – review & editing, Conceptualization, Supervision, Project administration, Visualization, Data curation, Validation, Resources. **Fatemeh Mohandes:** Investigation, Methodology.

Declaration of Competing Interest

The authors declare that they have no known competing financial interests or personal relationships that could have appeared to influence the work reported in this paper.

Acknowledgement

The authors are appreciative to Iran National Science Foundation (INSF, 99017572, 97017837) and the University of Kashan for funding this research by Grant No (159271/MG9).

References

- Aljohani, W., Ullah, M.W., Li, W., Shi, L., Zhang, X., Yang, G., 2018. Three-dimensional printing of alginate-gelatin-agar scaffolds using free-form motor assisted microsyringe extrusion system. *J. Polym. Res.* 25 (3), 62. <https://doi.org/10.1007/s10965-018-1455-0>.
- Al-Nayili, A., Albdiry, M., Salman, N., 2021. Dealumination of Zeolite Frameworks and Lewis Acid Catalyst Activation for Transfer Hydrogenation. *Arabian J. Sci. Eng.* 46, 5709–5716. <https://doi.org/10.1007/s13369-020-05312-w>.
- Al-Nayili, A., Albdiry, M., 2021. AuPd bimetallic nanoparticles supported on reduced graphene oxide nanosheets as catalysts for hydrogen generation from formic acid under ambient temperature. *New J. Chem.* 45, 10040–10048. <https://doi.org/10.1039/D1NJ01658J>.
- Amiri, B., Ghollassi, M., Shahrousvand, M., Kamali, M., Salimi, A., 2016. Osteoblast differentiation of mesenchymal stem cells on modified PES-PEG electrospun fibrous composites loaded with Zn₂SiO₄ bioceramic nanoparticles. *Differentiation* 92 (4), 148–158.
- Ardeshirylajimi, A., Hosseinkhani, S., Parivar, K., Yaghmaie, P., Soleimani, M., 2013. Nanofiber-based polyethersulfone scaffold and efficient differentiation of human induced pluripotent stem cells into osteoblastic lineage. *Mol. Biol. Rep.* 40 (7), 4287–4294.
- Balakrishnan, B., Jayakrishnan, A., 2005. Self-cross-linking biopolymers as injectable in situ forming biodegradable scaffolds. *Biomaterials* 26 (18), 3941–3951.
- Balakrishnan, B., Joshi, N., Jayakrishnan, A., Banerjee, R., 2014. Self-crosslinked oxidized alginate/gelatin hydrogel as injectable, adhesive biomimetic scaffolds for cartilage regeneration. *Acta Biomater.* 10 (8), 3650–3663.
- Bendtsen, S.T., Quinell, S.P., Wei, M., 2017. Development of a novel alginate-polyvinyl alcohol-hydroxyapatite hydrogel for 3D bioprinting bone tissue engineered scaffolds. *J. Biomed. Mater. Res. Part A* 105 (5), 1457–1468.
- Bendtsen, S.T., Wei, M., 2017. In vitro evaluation of 3D bioprinted tri-polymer network scaffolds for bone tissue regeneration. *J. Biomed. Mater. Res. Part A* 105 (12), 3262–3272.
- Bhardwaj, P., Singh, S., Singh, V., Aggarwal, S., Mandal, U.K., 2008. Nanosize polyacrylamide/SiO₂ composites by inverse microemulsion polymerization. *Int. J. Polym. Mater.* 57 (4), 404–416.
- Boyer, C., Figueiredo, L., Pace, R., Lesoeur, J., Rouillon, T., Visage, C.L., Tassin, J.-F., Weiss, P., Guicheux, J., Rethore, G., 2018. Laponite nanoparticle-associated silated hydroxypropylmethyl cellulose as an injectable reinforced interpenetrating network hydrogel for cartilage tissue engineering. *Acta Biomater.* 65, 112–122. <https://doi.org/10.1016/j.actbio.2017.11.027>.
- Chandra Babu, B., Rao, B.V., Ravi, M., Babu, S., 2017. Structural, microstructural, optical, and dielectric properties of Mn²⁺: Willemite Zn₂SiO₄ nanocomposites obtained by a sol-gel method. *J. Mol. Struct.* 1127, 6–14. <https://doi.org/10.1016/j.molstruc.2016.07.074>.
- Chen, G., Shen, D., Feng, M., Yang, M., 2004. An Attenuated Total Reflection FT-IR Spectroscopic Study of Polyamide 6/Clay Nanocomposite Fibers. *Macromol. Rapid Commun.* 25 (11), 1121–1124.
- Chen, H., Xing, X., Tan, H., Jia, Y., Zhou, T., Chen, Y., Ling, Z., Hu, X., 2017. Covalently antibacterial alginate-chitosan hydrogel dressing integrated gelatin microspheres containing tetracycline hydrochloride for wound healing. *Mater. Sci. Eng. C* 70, 287–295.
- D'Amora, U., Russo, T., De Santis, R., Gloria, A., Ambrosio, L., 2016. Hybrid nanocomposites with magnetic activation for advanced bone tissue engineering. In: *Bio-Inspired Regenerative Medicine: Materials, Processes, and Clinical Applications*, p. 179.
- D'Amora, U., Russo, T., Gloria, A., Riveccio, V., D'Antò, V., Negri, G., Ambrosio, L., De Santis, R., 2017. 3D additive-manufactured nanocomposite magnetic scaffolds: Effect of the application mode of a time-dependent magnetic field on hMSCs behavior. *Bioact. Mater.* 2 (3), 138–145. <https://doi.org/10.1016/j.bioactmat.2017.04.003>.
- Dai, X., Ma, C., Lan, Q., Xu, T., 2016. 3D bioprinted glioma stem cells for brain tumor model and applications of drug susceptibility. *Biofabrication* 8, (4) 045005.
- De Santis, R., D'Amora, U., Russo, T., Ronca, A., Gloria, A., Ambrosio, L., 2015. 3D fibre deposition and stereolithography techniques for the design of multifunctional nanocomposite magnetic scaffolds. *J. Mater. Sci. - Mater. Med.* 26 (10), 1–9.
- Dou, Q.Q., Liow, S.S., Ye, E., Lakshminarayanan, R., Loh, X.J., 2014. Biodegradable thermogelling polymers: working towards clinical applications. *Adv. Healthcare Mater.* 3 (7), 977–988.
- Emami, Z., Ehsani, M., Zandi, M., Daemi, H., Ghanian, M.-H., Foudazi, R., 2021. Modified hydroxyapatite nanoparticles reinforced nanocomposite hydrogels based on gelatin/oxidized alginate via Schiff base reaction. *Carbohydrate Polym. Technol. Applications* 2. <https://doi.org/10.1016/j.carpta.2021.100056>.
- Eslahi, N., Simchi, A., Mehrjoo, M., Shokrgozar, M.A., Bonakdar, S., 2016. Hybrid cross-linked hydrogels based on fibrous protein/block copolymers and layered silicate nanoparticles: tunable thermosen-

- sitivity, biodegradability and mechanical durability. *RSC Adv.* 6 (67), 62944–62957.
- Fan, L.H., Pan, X.R., Zhou, Y., Chen, L.Y., Xie, W.G., Long, Z.H., Zheng, H., 2011. Preparation and Characterization of Crosslinked Carboxymethyl Chitosan-Oxidized Sodium Alginate Hydrogels. *J. Appl. Polym. Sci.* 122 (4), 2331–2337. <https://doi.org/10.1002/app.34041>.
- Fu, P., Xu, K., Song, H., Chen, G., Yang, J., Niu, Y., 2010. Preparation, stability and rheology of polyacrylamide/pristine layered double hydroxide nanocomposites. *J. Mater. Chem.* 20 (19), 3869–3876.
- Ghanbari, M., Salavati-Niasari, M., Mohandes, F., 2021a. Injectable Hydrogels Based on Oxidized Alginate-Gelatin Reinforced by Carbon Nitride Quantum Dots for Tissue Engineering. *Int. J. Pharm.* 602. <https://doi.org/10.1016/j.ijpharm.2021.120660>
- Ghanbari, M., Salavati-Niasari, M., Mohandes, F., 2021b. Thermosensitive alginate–gelatin–nitrogen-doped carbon dots scaffolds as potential injectable hydrogels for cartilage tissue engineering applications. *RSC Adv.* 11 (30), 18423–18431.
- Ghanbari, M., Salavati-Niasari, M., Mohandes, F., Firouzi, Z., Mousavi, S.-D., 2021. The Impact of Zirconium Oxide Nanoparticles Content on Alginate Dialdehyde-Gelatin Scaffolds in Cartilage Tissue Engineering. *J. Mol. Liq.* 116531.
- Gheysari, H., Mohandes, F., Mazaheri, M., Dolatyar, B., Askari, M., Simchi, A., 2020. Extraction of Hydroxyapatite Nanostructures from Marine Wastes for the Fabrication of Biopolymer-Based Porous Scaffolds. *Mar. Drugs* 18 (1), 26.
- Gloria, A., Russo, T., D'Amora, U., Santin, M., De Santis, R., Ambrosio, L., 2020. Customised multiphasic nucleus/annulus scaffold for intervertebral disc repair/regeneration. *Connect. Tissue Res.* 61 (2), 152–162. <https://doi.org/10.1080/03008207.2019.1650037>.
- Hu, Z., Chen, G., 2014. Novel nanocomposite hydrogels consisting of layered double hydroxide with ultrahigh tensibility and hierarchical porous structure at low inorganic content. *Adv. Mater.* 26 (34), 5950–5956.
- Jamshidi Adegani, F., Langroudi, L., Ardashiryajimi, A., Dinarvand, P., Dodel, M., Doostmohammadi, A., Rahimian, A., Zohrabi, P., Seyedjafari, E., Soleimani, M., 2014. Coating of electrospun poly (lactic-co-glycolic acid) nanofibers with willemite bioceramic: improvement of bone reconstruction in rat model. *Cell Biol. Int.* 38 (11), 1271–1279.
- Jejurikar, A., Seow, X.T., Lawrie, G., Martin, D., Jayakrishnan, A., Grøndahl, L., 2012. Degradable alginate hydrogels crosslinked by the macromolecular crosslinker alginate dialdehyde [10.1039/C2JM30564J]. *J. Mater. Chem.* 22 (19), 9751–9758. <https://doi.org/10.1039/C2JM30564J>.
- Kadhem, A., Al-Nayili, A., 2021. Dehydrogenation of Formic Acid in Liquid Phase over Pd Nanoparticles Supported on Reduced Graphene Oxide Sheets. *Catal. Surv. Asia* 25, 324–333. <https://doi.org/10.1007/s10563-021-09332-w>.
- Karvandian, F.M., Shafiei, N., Mohandes, F., Dolatyar, B., Zandi, N., Zeynali, B., Simchi, A., 2020. Glucose cross-linked hydrogels conjugate HA nanorods as bone scaffolds: Green synthesis, characterization and in vitro studies. *Mater. Chem. Phys.* 242. <https://doi.org/10.1016/j.matchemphys.2019.122515>
- Ketabat, F., Karkhaneh, A., Mehdivavaz Aghdam, R., Hossein Ahmadi Tafti, S., 2017. Injectable conductive collagen/alginate/polypyrrole hydrogels as a biocompatible system for biomedical applications. *J. Biomater. Sci. Polym. Ed.* 28 (8), 794–805. <https://doi.org/10.1080/09205063.2017.1302314>.
- Khan, S., Ul-Islam, M., Ikram, M., Ullah, M.W., Israr, M., Subhan, F., Kim, Y., Jang, J.H., Yoon, S., Park, J.K., 2016. Three-dimensionally microporous and highly biocompatible bacterial cellulose–gelatin composite scaffolds for tissue engineering applications. *RSC Adv.* 6 (112), 110840–110849.
- Kosik-Kozioł, A., Costantini, M., Bolek, T., Szöke, K., Barbetta, A., Brinchmann, J., Świążkowski, W., 2017. PLA short sub-micron fiber reinforcement of 3D bioprinted alginate constructs for cartilage regeneration. *Biofabrication* 9, (4) 044105.
- Kundu, J., Shim, J.H., Jang, J., Kim, S.W., Cho, D.W., 2015. An additive manufacturing-based PCL–alginate–chondrocyte bioprinted scaffold for cartilage tissue engineering. *J. Tissue Eng. Regen. Med.* 9 (11), 1286–1297.
- LeBaron, R., Athanasiou, K., 2000. Ex vivo synthesis of articular cartilage. *Biomaterials* 21 (24), 2575–2587.
- Levental, I., Georges, P.C., Janmey, P.A., 2007. Soft biological materials and their impact on cell function [10.1039/B610522J]. *Soft Matter* 3 (3), 299–306. <https://doi.org/10.1039/B610522J>.
- Li, X., Wang, X., Wang, X., Chen, H., Zhang, X., Zhou, L., Xu, T., 2018. 3D bioprinted rat Schwann cell-laden structures with shape flexibility and enhanced nerve growth factor expression. *J. Biotech* 8 (8), 1–10.
- Lien, S.-M., Li, W.-T., Huang, T.-J., 2008. Genipin-crosslinked gelatin scaffolds for articular cartilage tissue engineering with a novel crosslinking method. *Mater. Sci. Eng., C* 28 (1), 36–43.
- Liow, S.S., Dou, Q., Kai, D., Karim, A.A., Zhang, K., Xu, F., Loh, X. J., 2016a. Thermogels In Situ Gelling Biomaterial. *ACS Biomater. Sci. Eng.* 2 (3), 295–316. <https://doi.org/10.1021/acsbiomaterials.5b00515>.
- Liow, S.S., Karim, A.A., Loh, X.J., 2016b. Biodegradable thermogelling polymers for biomedical applications. *MRS Bull.* 41 (7), 557–566. <https://doi.org/10.1557/mrs.2016.139>.
- Luo, Y., Lode, A., Akkineni, A.R., Gelinsky, M., 2015. Concentrated gelatin/alginate composites for fabrication of predesigned scaffolds with a favorable cell response by 3D plotting. *RSC Adv.* 5 (54), 43480–43488.
- Macaya, D., Ng, K.K., Spector, M., 2011. Injectable collagen–genipin gel for the treatment of spinal cord injury: in vitro studies. *Adv. Funct. Mater.* 21 (24), 4788–4797.
- Majidi, S.S., Slemming-Adamsen, P., Hanif, M., Zhang, Z., Wang, Z., Chen, M., 2018. Wet electrospun alginate/gelatin hydrogel nanofibers for 3D cell culture. *Int. J. Biol. Macromol.* 118, 1648–1654. <https://doi.org/10.1016/j.ijbiomac.2018.07.005>.
- Markstedt, K., Mantas, A., Tournier, I., Martínez Ávila, H. c., Hagg, D., & Gatenholm, P. (2015). 3D bioprinting human chondrocytes with nanocellulose–alginate bioink for cartilage tissue engineering applications. *Biomacromolecules*, 16(5), 1489–1496.
- Naghizadeh, Z., Karkhaneh, A., Khojasteh, A., 2018. Self-crosslinking effect of chitosan and gelatin on alginate based hydrogels: Injectable in situ forming scaffolds. *Mater. Sci. Eng., C* 89, 256–264. <https://doi.org/10.1016/j.msec.2018.04.018>.
- Nourafkan, E., Asachi, M., Gao, H., Raza, G., Wen, D., 2017. Synthesis of stable iron oxide nanoparticle dispersions in high ionic media. *J. Ind. Eng. Chem.* 50, 57–71.
- Ochi, M., Uchio, Y., Tobita, M., Kuriwaka, M., 2001. Current concepts in tissue engineering technique for repair of cartilage defect. *Artif. Organs* 25 (3), 172–179.
- Okay, O., Oppermann, W., 2007. Polyacrylamide–clay nanocomposite hydrogels: rheological and light scattering characterization. *Macromolecules* 40 (9), 3378–3387.
- Olubamiji, A.D., Zhu, N., Chang, T., Nwankwo, C.K., Izadifar, Z., Honaramooz, A., Chen, X., Eames, B.F., 2017. Traditional invasive and synchrotron-based noninvasive assessments of three-dimensional-printed hybrid cartilage constructs in situ. *Tissue Engineering Part C: Methods* 23 (3), 156–168.
- Park, J., Lee, S.J., Lee, H., Park, S.A., Lee, J.Y., 2018. Three dimensional cell printing with sulfated alginate for improved bone morphogenetic protein-2 delivery and osteogenesis in bone tissue engineering. *Carbohydr. Polym.* 196, 217–224.
- Purohit, S.D., Singh, H., Bhaskar, R., Yadav, I., Bhushan, S., Gupta, M.K., Kumar, A., Mishra, N.C., 2020. Fabrication of graphene oxide and nanohydroxyapatite reinforced gelatin–alginate

- nanocomposite scaffold for bone tissue regeneration. *Front. Mater* 7, 1–10.
- Radhakrishnan, A., Jose, G.M., Kurup, M., 2015. PEG-penetrated chitosan–alginate co-polysaccharide-based partially and fully cross-linked hydrogels as ECM mimic for tissue engineering applications. *Prog. Biomater.* 4 (2), 101–112. <https://doi.org/10.1007/s40204-015-0041-3>.
- Rahaman, M.N., Day, D.E., Bal, B.S., Fu, Q., Jung, S.B., Bonewald, L.F., Tomsia, A.P., 2011. Bioactive glass in tissue engineering. *Acta Biomater.* 7 (6), 2355–2373.
- Rogalsky, A.D., Kwon, H.J., Lee-Sullivan, P., 2011. Compressive stress–strain response of covalently crosslinked oxidized-alginate/N-succinyl-chitosan hydrogels. *J. Biomed. Mater. Res. Part A* 99 (3), 367–375.
- Sarker, B., Singh, R., Zehnder, T., Forger, T., Alexiou, C., Cicha, I., Detsch, R., Boccaccini, A.R., 2017. Macromolecular interactions in alginate–gelatin hydrogels regulate the behavior of human fibroblasts. *J. Biactive Compatible Polym.* 32 (3), 309–324.
- Sergi, R., Bellucci, D., & Cannillo, V., 2020. A Review of Bioactive Glass/Natural Polymer Composites: State of the Art. *Materials*, 13 (23), 5560. <https://www.mdpi.com/1996-1944/13/23/5560>
- Shim, J.-H., Lee, J.-S., Kim, J.Y., Cho, D.-W., 2012. Bioprinting of a mechanically enhanced three-dimensional dual cell-laden construct for osteochondral tissue engineering using a multi-head tissue/organ building system. *J. Micromech. Microeng.* 22, (8) 085014.
- Tan, H., Fan, M., Ma, Y., Qiu, J., Li, X., Yan, J., 2014. Injectable gel scaffold based on biopolymer microspheres via an enzymatic reaction. *Adv. Healthcare Mater.* 3 (11), 1769–1775.
- Tan, H., Gao, X., Sun, J., Xiao, C., Hu, X., 2013. Double stimulus-induced stem cell aggregation during differentiation on a biopolymer hydrogel substrate. *Chem. Commun.* 49 (98), 11554–11556.
- Tan, H., Shen, Q., Jia, X., Yuan, Z., Xiong, D., 2012. Injectable nanohybrid scaffold for biopharmaceuticals delivery and soft tissue engineering. *Macromol. Rapid Commun.* 33 (23), 2015–2022.
- Temenoff, J.S., Mikos, A.G., 2000. Tissue engineering for regeneration of articular cartilage. *Biomaterials* 21 (5), 431–440.
- Tjong, S.C., 2006. Structural and mechanical properties of polymer nanocomposites. *Mater. Sci. Eng. R Rep.* 53 (3–4), 73–197.
- Ul-Islam, M., Khan, T., Park, J.K., 2012. Water holding and release properties of bacterial cellulose obtained by in situ and ex situ modification. *Carbohydr. Polym.* 88 (2), 596–603.
- Urruela-Barrios, R., Ramírez-Cedillo, E., Díaz de León, A., Alvarez, A.J., Ortega-Lara, W., 2019. Alginate/gelatin hydrogels reinforced with TiO₂ and β -TCP fabricated by microextrusion-based printing for tissue regeneration. *Polymers* 11 (3), 457.
- Vieira, E.F.S., Cestari, A.R., Airoidi, C., Loh, W., 2008. Polysaccharide-Based Hydrogels: Preparation, Characterization, and Drug Interaction Behaviour. *Biomacromolecules* 9 (4), 1195–1199. <https://doi.org/10.1021/bm7011983>.
- Wang, Q., Hou, R., Cheng, Y., Fu, J., 2012. Super-tough double-network hydrogels reinforced by covalently compositing with silicnanoparticles. *Soft Matter* 8 (22), 6048–6056.
- Wu, Y.-L., Wang, H., Qiu, Y.-K., Loh, X.J., 2016. PLA-based thermogel for the sustained delivery of chemotherapeutics in a mouse model of hepatocellular carcinoma. *RSC Adv.* 6 (50), 44506–44513.
- Yan, J., Miao, Y., Tan, H., Zhou, T., Ling, Z., Chen, Y., Xing, X., Hu, X., 2016. Injectable alginate/hydroxyapatite gel scaffold combined with gelatin microspheres for drug delivery and bone tissue engineering. *Mater. Sci. Eng. C* 63, 274–284. <https://doi.org/10.1016/j.msec.2016.02.071>.
- Yan, S., Wang, T., Feng, L., Zhu, J., Zhang, K., Chen, X., Cui, L., Yin, J., 2014. Injectable in situ self-cross-linking hydrogels based on poly (L-glutamic acid) and alginate for cartilage tissue engineering. *Biomacromolecules* 15 (12), 4495–4508.
- Yang, X., Lu, Z., Wu, H., Li, W., Zheng, L., Zhao, J., 2018. Collagen-alginate as bioink for three-dimensional (3D) cell printing based cartilage tissue engineering. *Mater. Sci. Eng., C* 83, 195–201.
- Zaragoza, J., & Asuri, P. (2019). Exploring the Effects of Nanoparticle Incorporation on the Mechanical Properties of Hydrogels. *Proceedings*, 3(1), 2. <https://www.mdpi.com/2504-3900/3/1/2>
- Zhang, L., Tao, T., Li, C., 2009. Formation of polymer/carbon nanotubes nano-hybrid shish–kebab via non-isothermal crystallization. *Polymer* 50 (15), 3835–3840.